HHS Public Access

Author manuscript

*Adv Mater*. Author manuscript; available in PMC 2017 January 01.

Published in final edited form as:

*Adv Mater*. 2015 August ; 27(30): 4481–4486. doi:10.1002/adma.201501156.

# Identifying and Eliminating Emissive Sub-bandgap States in Thin Films of PbS Nanocrystals

**Gyu Weon Hwang**,
Department of Materials Science and Engineering, Massachusetts Institute of Technology, Cambridge, MA 02139, USA

**Donghun Kim**,
Department of Materials Science and Engineering, Massachusetts Institute of Technology, Cambridge, MA 02139, USA

**Jose M. Cordero**,
Department of Chemistry, Massachusetts Institute of Technology, Cambridge MA 02139, USA

**Dr. Mark W. B. Wilson**,
Department of Chemistry, Massachusetts Institute of Technology, Cambridge MA 02139, USA

**Chia-Hao M. Chuang**,
Department of Materials Science and Engineering, Massachusetts Institute of Technology, Cambridge, MA 02139, USA

**Prof. Jeffrey C. Grossman**, and
Department of Materials Science and Engineering, Massachusetts Institute of Technology, Cambridge, MA 02139, USA

**Prof. Moungi G. Bawendi**
Department of Chemistry, Massachusetts Institute of Technology, Cambridge MA 02139, USA

The size-dependent bandgap tunability and solution process-ability of quantum dots (QDs) make them attractive candidates for optoelectronic applications.[1–7] QDs have been actively explored for applications as light emitting diodes,[7,8] photodetectors,[2,9,10] and photovoltaics.[1,5,11,12] However, further improvements in device performance are required to make them competitive.[11,13–17] One well-known factor that presently limits the device performance of QD thin films is sub-bandgap states, also referred to as trap states,[16–19] which have been observed using optical field effect transistors and scanning tunneling spectroscopy.[20,21] These states, for instance, are thought to give rise to the open-circuit voltage deficit in photovoltaic applications[22,23] and cause a drastic decrease of charge carrier lifetimes and diffusion lengths.[13,17,24] A common view is that trap states are sub-bandgap surface states caused by dangling bonds or unpassivated surface atoms.[14,18,25–27] Thus, previous approaches to reduce the density of traps have included attempts to exchange the binding groups of passivating ligands,[1,14,27] increase the ligand coverage,[14,28] or

Correspondence to: Moungi G. Bawendi.

Supporting Information

Supporting Information is available from the Wiley Online Library or from the author.

balance the stoichiometry at the dot surfaces.[29] Recently, Carey and coworkers demonstrated that sub-bandgap emission from PbS QD films treated with 3-mercaptopropionic acid (MPA) can be removed by further treatment with acidic solutions, especially pyruvic acid.[19] Even though these treatments led to improved device performance, the lack of a fundamental understanding of the mechanism has impaired efforts to control trap states in general and, thereby, improve device performance. Here, we use X-ray photoelectron spectroscopy (XPS) and density functional theory (DFT) calculations to identify chemically reduced (or under-charged) Pb atoms as the origin of trap states in ligand-exchanged PbS QD thin films. We then use chemical oxidation to achieve a 40-fold reduction in the density of trap states by controlling the oxidation states of Pb atoms. Our discovery of a chemical origin for the trap states in PbS films offers an opportunity to rationally control their density, and thereby to fabricate improved devices.

PbS QD thin films have been researched intensively for optoelectronic applications due to a tunable bandgap energy that covers the ideal range used for photovoltaics and optical communications in the near infrared and short-wavelength infrared,[5,7,8,30] as well as the availability of a straightforward, scalable synthesis.[31] As-synthesized (see the Experimental Section), the QDs have bulky organic ligands, so it is generally necessary to exchange these with smaller molecules to facilitate charge transport.[1–3,14] Typical ligands used for the fabrication of QD devices include: 1,2-ethanedithiol (EDT), MPA, tetrabutylammonium iodide (TBAI), and n-butylamine (nBA).

We prepare EDT-, MPA-, and TBAI-treated PbS films by conventional solid-state ligand exchange procedures[1,11–15,27,32] and nBA-treated samples by an established solution-phase ligand exchange procedure.[33] As seen in Figure 1a, photoluminescence (PL) measurements show that additional sub-bandgap emission is observed following every ligand exchange process—independent of the binding group of the ligands. In detail, PbS QDs with native oleic acid ligands (OA, black) show only band edge emission at ≈1050 nm. By contrast, EDT (blue)-, TBAI (green)-, and nBA (red)-treated samples show broad, but distinct emission peaks near 1500, 1600, and 1400 nm, respectively, and the MPA-treated sample (orange) shows a long red tail. All these additional emissive features reside at lower energies than the band edge emission, which indicates that the newly formed emissive states are located inside the bandgap. For the nBA-treated sample, we note that band edge emission near 1100 nm is considerably weaker than the trap emission, while the band edge emission for all ligand-exchanged samples are slightly redshifted due to the increased dielectric environments and altered diffusion of photo-excitations induced by the shorter dot-to-dot distance.[34–36]

To identify whether a chemical species is associated with this trap emission, we performed high-resolution XPS on each film, focusing on the Pb 4f spectral feature to obtain information on the bonding character of the Pb atoms (Figure 1b). The expected spectral positions for three species[37] are high-lighted with colored bands: metallic Pb as tan, Pb—S as blue, and Pb—carboxylate as gray. Peak locations for Pb bonded to other ligands are not explicitly marked since these features are not prominent in our data and are covered under the tails of Pb—S peaks. Before ligand exchange, the OA-coated film shows a single, relatively broad feature due to the overlap between the two peaks from Pb–S and Pb—

carboxylates. The deconvoluted spectrum of the OA-coated QD film is shown in Figure S2 (Supporting Information).

After ligand exchange, we observe that the Pb—carboxylate features are diminished for all samples, and an additional peak evolves with a lower binding energy than either Pb—S or Pb—carboxylate bonds. The new peak corresponds to the binding energy of metallic Pb,[37] which indicates that a few $Pb^{2+}$ atoms in Pb—S bonds have been chemically reduced to have less charge than regular Pb—S bonds. The consistent trend in our XPS results for each ligand implies that these additional emissive trap states are from reduced or "under-charged" Pb atoms.

To verify whether the formation of under-charged Pb atoms contributes to the emissive sub-bandgap states, we oxidized the ligand-exchanged films with a mild oxidizing agent, 1,4-benzoquinone (BQ). As shown in Figure 1c, XPS measurements confirm that the BQ treatment successfully removes the undercharged Pb atoms. Further, after oxidation, all ligand-exchanged PbS QD films exhibit only band edge emission, as shown in Figure 1d. This additional BQ treatment induces a modest (10%–40%) decrease of the PL intensity relative to the ligand-exchanged films, with some dependence on processing conditions. Additional XPS results shown in Figure S4 (Supporting Information) demonstrate that this effect can be achieved with other oxidation methods, such as pyruvic acid treatment and annealing in air. These results all support a causal relationship between under-charged Pb and emissive trap states.

It is important to ensure that the removal of the emissive sub-bandgap states by BQ treatment is not due to an additional ligand exchange or a change in the ligand coverage. Compared to sulfur- and nitrogen-bearing ligands, TBAI-treated PbS QDs have the convenient property that the elemental signature of I is readily distinguishable in XPS experiments. As shown in Table 1, XPS measurements on TBAI-treated PbS QDs confirm that the I-to-Pb ratio remains constant after BQ treatment, which verifies that the ligand binding on QDs remains intact after the BQ treatment.

To test the possibility that under-charged Pb atoms can form under these conditions and give rise to sub-bandgap states, we calculate the electronic structure of a PbS QD using DFT. For the study, we construct a model QD based on the elemental composition of TBAI-treated QDs, which is measured by wavelength dispersive spectroscopy (WDS) and XPS (Table 1). The Pb-to-S ratio determines the proportion between stoichiometric (100) facets and Pb-terminated (111) facets in a truncated octahedron shape. The final QD used for simulations is 1.95 nm in diameter and consists of 116 Pb atoms, 79 S atoms, and 35 I atoms (Figure 2a). We focus on QDs with iodide ($I^-$) ligands as they are used in modern, high-performance photovoltaic devices,[11] and the simple structure reduces the computational burden, allowing the simulation of larger QDs.

Using this model QD, a Bader charge analysis on the DFT calculation shows the existence of the under-charged Pb atoms. Bader charge analysis is a post-processing method which can partition the continuous charge density along the whole system obtained from DFT so that local charges of individual atoms can be determined.[38] Figure 2b shows the charge

distribution (i.e., the atom population density versus local charge) of each atomic species in the constructed particle. For Pb atoms, a major peak in population density is observed at +0.90 (in units of electron charge) with weaker, broader features at lower levels of charge (+0.4 to +0.75). These broad features in lower ranges indicate the existence of stable, under-charged Pb atoms, which is consistent with our experimental observations using XPS. In comparison, the S atoms and I atoms have single, narrow peaks at −0.90 and at −0.5 electron charges, respectively. We note that these values are less than the formal valence charge because the bonds have mixed covalent/ionic nature. For example, as shown in Figure S5 (Supporting Information), Pb and S atoms in PbS bulk possess a local charge of about +0.95 and −0.95, respectively.

Figure 2c,d shows the density of states (DoS) for our model QD calculated using DFT. The total DoS (black) reflects all available electronic states and is broken down into a projected density of states (PDoS) for each atomic species, S (orange), I (purple), and Pb (blue). The PDoS of Pb atoms is further subdivided into contributions from regular-charged (green) and under-charged Pb atoms (red). We define under-charged Pb atoms as those having a charge less than 0.8 electron charges. This threshold value was suggested by the profile of the atomic population density for Pb in Figure 2b and supported by additional Bader charge calculations that showed that neither bulk PbS, nor stoichiometric and sulfur-rich QDs have features in this region (Figure S5, Supporting Information). Returning to the PDoS in Figure 2d, it is clear that the density of states inside the bandgap arises overwhelmingly from under-charged Pb atoms (<0.8), which is in good agreement with our conclusions from the PL and XPS results shown in Figure 1. This is an important refinement over a simple “dangling bond” picture. Additional calculations (Figure S6, Supporting Information) on “bare” QDs —where all surface Pb atoms have dangling bonds—show that only Pb atoms on (111) surfaces are under-charged and contribute to sub-bandgap states, while Pb atoms on (100) surface are not under-charged and do not contribute to sub-bandgap states.

Our calculations allow us to investigate the effect of ligands on the electronic structure of off-stoichiometric (lead-rich) PbS QDs and provide a fundamental explanation of previous approaches to control trap states with ligand treatments.[14,24,26,27,29,32] As we (Table 1) and others[39,40] have shown, as-synthesized PbS QDs tend to be lead rich. The excess Pb atoms are located on the off-stoichiometric (111) surface (Figure S6, Supporting Information) and calculations on bare (ligand-free) QDs show that overall charge balance is maintained by the under-charged Pb atoms (Figure S7, Supporting Information). However, as shown in Figure S8 (Supporting Information), the addition of iodine ligands decreases the number of under-charged Pb atoms by contributing partial negative charge. This is consistent with a previous theoretical study that indicates that the level of the suppression depends on ligand coverage.[28] However, we note that this cancellation is not expected to be exact under most conditions used in device fabrications.[11,19,22,29] Instead, because the electronegativity of the binding groups determines the amount of partial charge that can be donated, different types of ligands are expected to yield different levels of suppression (Figure S9a, Supporting Information) and a different profile of sub-bandgap states (Figure S9b, Supporting Information). This provides a rationale for the many studies showing that ligands affect the electronic structure and Fermi level of QD thin films.[28,32,41–44]

Finally, we employ electrical measurements to demonstrate that BQ treatment effectively removes electrically active trap states and does not simply suppress the spectroscopically observed trap emission by causing the trap states to become wholly non-radiative. We measure the density of trap states using drive-level capacitance profiling (DLCP), a technique originally developed for materials possessing a large number of defects, such as amorphous silicon and polycrystalline $CuIn_xGa_{1-x}Se_2$.[45,46] DLCP was chosen over commonly used deep-level transient spectroscopy (DLTS) because conventional DLTS can be only used for materials with sufficiently low defect concentrations to ensure the exponential decay of capacitance,[16,47–49] and QD films are known to have a larger density of traps than the density of free carriers.[15,25,47] In DLCP, the density of trap states is measured by analyzing the capacitance response—which depends on the depletion width in Schottky diodes—at different modulation amplitudes and frequencies. Conductive and trap states can be distinguished by their frequency responses. Under high-frequency modulation, only free carriers in conductive states contribute to the capacitance because carriers do not have enough time to interact significantly with trap states. By contrast, in the low-frequency regime, carriers do have enough time to occupy and detrap from sub-bandgap states, so both conductive and trap states contribute to the capacitance. The threshold frequency where carriers start interacting with trap states is determined by the characteristic energy level of the trap states and the temperature.[45]

The structure of Schottky diodes used in the DLCP measurement is shown in Figure 3a. We compare density of trap states of EDT-treated PbS QD films with and without BQ treatment and present our results in Figure 3b. Prior to BQ treatment, we observe that there is a much greater density of available states at low modulation frequencies compared to the high-frequency regime, which is consistent with the presence of trap states. We find that the absolute density of trap states is $4.8 \times 10^{16}$ $cm^{-3}$ ($\approx 2.7 \times 10^{-3}$ $dot^{-1}$), which is in agreement with values measured using other methods.[15,47] After oxidation, we observe that the low-frequency feature is strongly diminished and our analysis shows a 40-fold decrease of trap density to $1.2 \times 10^{15}$ $cm^{-3}$ —a level of suppression that is expected to yield a sixfold improvement in the carrier diffusion length.[17] Therefore, we conclude not only that oxidation by BQ effectively reduces the density of trap states but also that the emissive sub-bandgap states induced by ligand exchange are electrically active. Further, we rule out the alternative explanation that oxidation by BQ only suppresses trap emission by rendering the states totally non-radiative—the DLCP results show that the sub-bandgap states have been removed.

However, it appears that this BQ treatment also has other, more subtle, effects on the films. Examining the high-frequency region of the DLCP measurements presented in Figure 3b, we observe that the treatment leads to an increase in the density of intrinsic free carriers. This suggests that the treatment may alter the dynamics of spontaneous (thermally activated) carrier generation, which may influence the fate of photoexcited excitons. We consider that this effect may be partially responsible for the 10–40% decrease in the time-integrated photoluminescence quantum yield of films following treatment, although further experiments will be required to reveal the respective roles of geminate, bimolecular, and trap-assisted recombination dynamics in these films.

In this paper, we have identified the chemical origin of sub-bandgap states in ligand-exchanged PbS QD thin films using a combined experimental/theoretical approach. We show experimentally that under-charged Pb atoms result from ligand exchange and are associated with sub-bandgap states that are both optically and electrically active. Theoretical calculations using DFT and Bader charge analysis confirm that under-charged Pb atoms give rise to sub-bandgap states. We discover that treatment with BQ reoxidizes these undercharged Pb atoms and suppresses trap emission and then use DLCP to show quantitatively that it achieves 40-fold decrease in the density of trap states. We expect that insights developed in this paper on the fundamental origin of trap formation will provide direction for controlling the density of trap states in thin films of QDs and thereby improve the performance of QD devices.

## Experimental Section

### Sample Preparation

Synthesis and fabrication procedures are performed under nitrogen atmosphere using Schlenk line techniques and gloveboxes. OA-capped PbS QDs are synthesized using a literature method[11,31] and purified three times by precipitation in a mixture of ethanol and 1-butanol, followed by centrifugation and resuspension in hexane. OA-capped QD and nBA treated QDs are drop-cast to form a film. Solution-phase ligand exchange of nBA is performed by the following steps: After a further precipitation, PbS QDs are dissolved into nBA with a concentration of 25 mg $mL^{-1}$ and the solution is stirred overnight. Films are fabricated by drop-casting. QD solutions at a concentration of 50 mg $mL^{-1}$ in octane are used for spin-casting. EDT, TBAI, and MPA treated QD films are prepared by sequential spin-casting. For each layer, 20 μL of QD solution is spin-cast at 1500 rpm for 30 s on a Si substrate. Roughly 0.1 mL of ligand solution is then dispensed onto the substrate, allowed to sit for 30 s, and spun dry. The substrate is then washed with the excess solvent used for ligand exchange and spun dry three times to remove unbound ligands and the entire process is repeated; each complete iteration results in the deposition of ≈20 nm of QDs. The ligand concentrations and solvents used in this study are EDT 0.02% (v/v) in acetonitrile, TBAI 10 mg $mL^{-1}$ in methanol, and MPA 1% (v/v) in methanol. For the selected films, the oxidation process is performed between layer depositions. Roughly 0.1 mL of 10 mg $mL^{-1}$ BQ solution in methanol is dispensed onto the ligand-exchanged films, allowed to sit for 30 s, and spun dry followed by three sequential washes with methanol.

### Characterization

PL measurements were conducted at a room temperature with 532 nm diode laser excitation. [3.0 mW into a ≈135 μm spot ($1/e^2$ diameter) for an irradiance of ≈150 mW $cm^{-2}$] The photoluminescence was collected using reflective optics, passed through a long-pass filter (3 mm Schott RG780) to remove pump scatter, spectrally dispersed using an Acton 300i spectrometer, and measured using an InGaAs array detector (Roper Scientific). XPS measurements were performed using a PHI Versaprobe II X-ray Photoelectron Spectrometer and the spectra were analyzed using CasaXPS software. WDS measurements were performed using a JEOL JXA-8200 SuperProbe. DLCP measurement was performed using a Solartron 1260 impedance analyzer, in a nitrogen glove box.

### Density Functional Theory Calculations

DFT calculations were performed using the Vienna ab initio simulation packages (VASP)[50] with the generalized gradient approximation of Perdew–Burke–Ernzerhof (PBE)[51] for the exchange and correlation functional. The projector-augmented-wave method was adopted to describe the core electrons. An energy cutoff of 400 eV and a Monkhorst–Pack *k*-point sampling of 1 × 1 × 1 were used. A large vacuum spacing of >15 Å was used to prevent spurious inter-QD interactions. PbS QDs bearing iodine ligand were fully relaxed using the conjugate gradient method until the structure satisfied the following relaxation criteria: i) the energy difference between two consecutive ionic steps is less than $10^{-4}$ eV and ii) the maximum Hellmann–Feynman forces acting on each atom are less than 0.01 eV $Å^{-1}$. Bader charge analysis was postperformed on charge density results obtained from DFT in order to calculate local charge that each atom in a QD possess.[38]

## Supplementary Material

Refer to Web version on PubMed Central for supplementary material.

## Acknowledgments

The authors gratefully acknowledge Dr. H.-S. Han, J. M. Scherer, D. Ko, and I. Coropceanu for insightful discussions and technical assistance as well as Dr. N. Chatterjee for WDS measurements. The authors thank the National Energy Research Scientific Computing (NERSC) for computing resources. This work made use of the MRSEC Shared Experimental Facilities at MIT, supported by the National Science Foundation under Award No. DMR-08-19762. This work was supported in part by the U.S. Army Research Laboratory and the U.S. Army Research Office through the Institute for Soldier Nanotechnologies, under Contract No. W911NF-13-D-0001, and by the Samsung Advanced Institute of Technology. D.K. acknowledges support from the Samsung Scholarship Foundation. M.W.B.W. acknowledges partial support from the excitonic EFRC at MIT, an Energy Frontier Research Center funded by the U.S. Department of Energy (DOE), Office of Science, Basic Energy Sciences (BES), under Award No. DE-SC0001088. Part of this work made use of the MIT Laser Biomedical Research Center (LBRC) under contract number 9-P41-EB015871-26A1, supported by the National Institute of Health.

## References

1. Kim JY, Voznyy O, Zhitomirsky D, Sargent EH. Adv. Mater. 2013; 25:4986. [PubMed: 24002864]
2. Konstantatos G, Sargent EH. Nat. Nanotechnol. 2010; 5:391. [PubMed: 20473301]
3. Kramer IJ, Sargent EH. Chem. Rev. 2014; 114:863. [PubMed: 24053639]
4. Talapin DV. MRS Bull. 2012; 37:63.
5. Tang J, Sargent EH. Adv. Mater. 2011; 23:12. [PubMed: 20842658]
6. Kovalenko MV, Manna L, Cabot A, Hens Z, Talapin DV, Kagan CR, Klimov VI, Rogach AL, Reiss P, Milliron DJ, Guyot-Sionnnest P, Konstantatos G, Parak WJ, Hyeon T, Korgel BA, Murray CB, Heiss W. ACS Nano. 2015; 9:1012. [PubMed: 25608730]
7. Shirasaki Y, Supran GJ, Bawendi MG, Bulovic V. Nat. Photonics. 2013; 7:13.
8. Supran GJ, Song KW, Hwang GW, Correa RE, Scherer J, Dauler EA, Shirasaki Y, Bawendi MG, Bulović V. Adv. Mater. 2015; 27:1437. [PubMed: 25639896]
9. Clifford J, Konstantatos G. Nat. Nanotechnol. 2008; 4:40. [PubMed: 19119281]
10. Geyer SM, Scherer JM, Moloto N, Jaworski FB, Bawendi MG. ACS Nano. 2011; 5:5566. [PubMed: 21591692]
11. Chuang C-HM, Brown PR, Bulović V, Bawendi MG. Nat. Mater. 2014; 13:796. [PubMed: 24859641]
12. Chang L-Y, Lunt RR, Brown PR, Bulović V, Bawendi MG. Nano Lett. 2013; 13:994. [PubMed: 23406331]

13. Zhitomirsky D, Voznyy O, Hoogland S, Sargent EH. ACS Nano. 2013; 7:5282. [PubMed: 23701285]
14. Ip AH, Thon SM, Hoogland S, Voznyy O, Zhitomirsky D, Debnath R, Levina L, Rollny LR, Carey GH, Fischer A, Kemp KW, Kramer IJ, Ning Z, Labelle AJ, Chou KW, Amassian A, Sargent EH. Nat. Nanotechnol. 2012; 7:577. [PubMed: 22842552]
15. Wanger DD, Correa RE, Dauler EA, Bawendi MG. Nano Lett. 2013; 13:5907. [PubMed: 24256125]
16. Bozyigit D, Wood V. J Mater. Chem. C. 2014; 2:3172.
17. Zhitomirsky D, Voznyy O, Levina L, Hoogland S, Kemp KW, Ip AH, Thon SM, Sargent EH. Nat. Commun. 2014; 5:3803. [PubMed: 24801435]
18. Stadler P, Sutherland BR, Ren Y, Ning Z, Simchi A, Thon SM, Hoogland S, Sargent EH. ACS Nano. 2013; 7:5757. [PubMed: 23786265]
19. Carey GH, Kramer IJ, Kanjanaboos P, Moreno-bautista G, Voznyy O, Rollny L, Tang JA, Hoogland S, Sargent EH. ACS Nano. 2014; 8:11763. [PubMed: 25376698]
20. Nagpal P, Klimov VI. Nat. Commun. 2011; 2:486. [PubMed: 21952220]
21. Diaconescu B, Padilha LA, Nagpal P, Swartzentruber BS, Klimov VI. Phys. Rev. Lett. 2013; 110:127406. [PubMed: 25166850]
22. Chuang C-HM, Maurano A, Brandt RE, Hwang GW, Jean J, Buonassisi T, Bulović V, Bawendi MG. Nano Lett. 2015; 15:3286. [PubMed: 25927871]
23. Bozyigit D, Lin WMM, Yazdani N, Yarema O, Wood V. Nat. Commun. 2015; 6:6180. [PubMed: 25625647]
24. Jeong KS, Tang J, Liu H, Kim J, Schaefer AW, Kemp K, Levina L, Wang X, Hoogland S, Debnath R, Brzozowski L, Sargent EH, Asbury JB. ACS Nano. 2012; 6:89. [PubMed: 22168594]
25. Bozyigit D, Volk S, Yarema O, Wood V. Nano Lett. 2013; 13:5284. [PubMed: 24164600]
26. Klem EJD, Shukla H, Hinds S, MacNeil DD, Levina L, Sargent EH. Appl. Phys. Lett. 2008; 92:212105.
27. Ning Z, Ren Y, Hoogland S, Voznyy O, Levina L, Stadler P, Lan X, Zhitomirsky D, Sargent EH. Adv. Mater. 2012; 24:6295. [PubMed: 22968838]
28. Kim D, Kim DH, Lee JH, Grossman JC. Phys. Rev. Lett. 2013; 110:196802. [PubMed: 23705733]
29. Oh SJ, Berry NE, Choi J-H, Gaulding EA, Paik T, Hong S-H, Murray CB, Kagan CR. ACS Nano. 2013; 7:2413. [PubMed: 23368728]
30. Graetzel M, Janssen RAJ, Mitzi DB, Sargent EH. Nature. 2012; 488:304. [PubMed: 22895335]
31. Hines MA, Scholes GD. Adv. Mater. 2003; 15:1844.
32. Brown PR, Kim D, Lunt RR, Zhao N, Bawendi MG, Grossman JC, Bulović V. ACS Nano. 2014; 8:5863. [PubMed: 24824726]
33. Mentzel TS, Wanger DD, Ray N, Walker BJ, Strasfeld D, Bawendi MG, Kastner MA. Nano Lett. 2012; 12:4404. [PubMed: 22784104]
34. Guyot-Sionnest P. J Phys. Chem. Lett. 2012; 3:1169. [PubMed: 26288053]
35. Gao J, Johnson JC. ACS Nano. 2012; 6:3292. [PubMed: 22462777]
36. Gao J, Zhang J, van de Lagemaat J, Johnson JC, Beard MC. ACS Nano. 2014; 8:12814. [PubMed: 25485555]
37. a) Moulder, JF., Stickle, WF., Sobol, PE., Bomben, KD. Handbook of X-Ray Photoelectron Spectroscopy. Perkin–Elmer Corporation; Eden Prairie, MN: 1992. b) NIST X-ray Photoelectron Spectroscopy Database, Version 4.1 (2012). Gaithersburg, MD, USA: National Institute of Standards and Technology; http://srdata.nist.gov/xps/ [accessed: February 2015]
38. Henkelman G, Arnaldsson A, Jónsson H. Comput. Mater. Sci. 2006; 36:354.
39. Choi H, Ko JH, Kim YH, Jeong S. J Am. Chem. Soc. 2013; 135:5278. [PubMed: 23496143]
40. Justo Y, Sagar LK, Flamee S, Zhao Q, Vantomme A, Hens Z. ACS Nano. 2014; 8:7948. [PubMed: 25090034]
41. Voznyy O, Zhitomirsky D, Stadler P, Ning Z, Hoogland S, Sargent EH. ACS Nano. 2012; 6:8448. [PubMed: 22928602]
42. Voznyy O, Thon SM, Ip AH, Sargent EH. J Phys. Chem. Lett. 2013; 4:987. [PubMed: 26291365]

43. Giansante C, Infante I, Fabiano E, Grisorio R, Suranna GP, Gigli G. J Am. Chem. Soc. 2015; 137:1875. [PubMed: 25574692]
44. Frederick MT, Amin VA, Weiss EA. J Phys. Chem. Lett. 2013; 4:634. [PubMed: 26281879]
45. Heath JT, Cohen JD, Shafarman WN. J Appl. Phys. 2004; 95:1000.
46. Michelson CE, Gelatos AV, Cohen JD. Appl. Phys. Lett. 1985; 47:412.
47. Bozyigit D, Jakob M, Yarema O, Wood V. ACS Appl. Mater. Interfaces. 2013; 5:2915. [PubMed: 23527751]
48. Blood, P., Orton, JW. The Electrical Characterization of Semiconductors: Majority Carriers and Electron States. San Diego, CA, USA: Academic Press; 1992.
49. Schroder, DK. Semiconductor Material and Device Characterization. Hoboken, NJ, USA: John Wiley & Sons, Inc; 2006.
50. Kresse G, Furthmüller J. Comput. Mater. Sci. 1996; 6:15.
51. Perdew JP, Burke K, Ernzerhof M. Phys. Rev. Lett. 1996; 77:3865. [PubMed: 10062328]

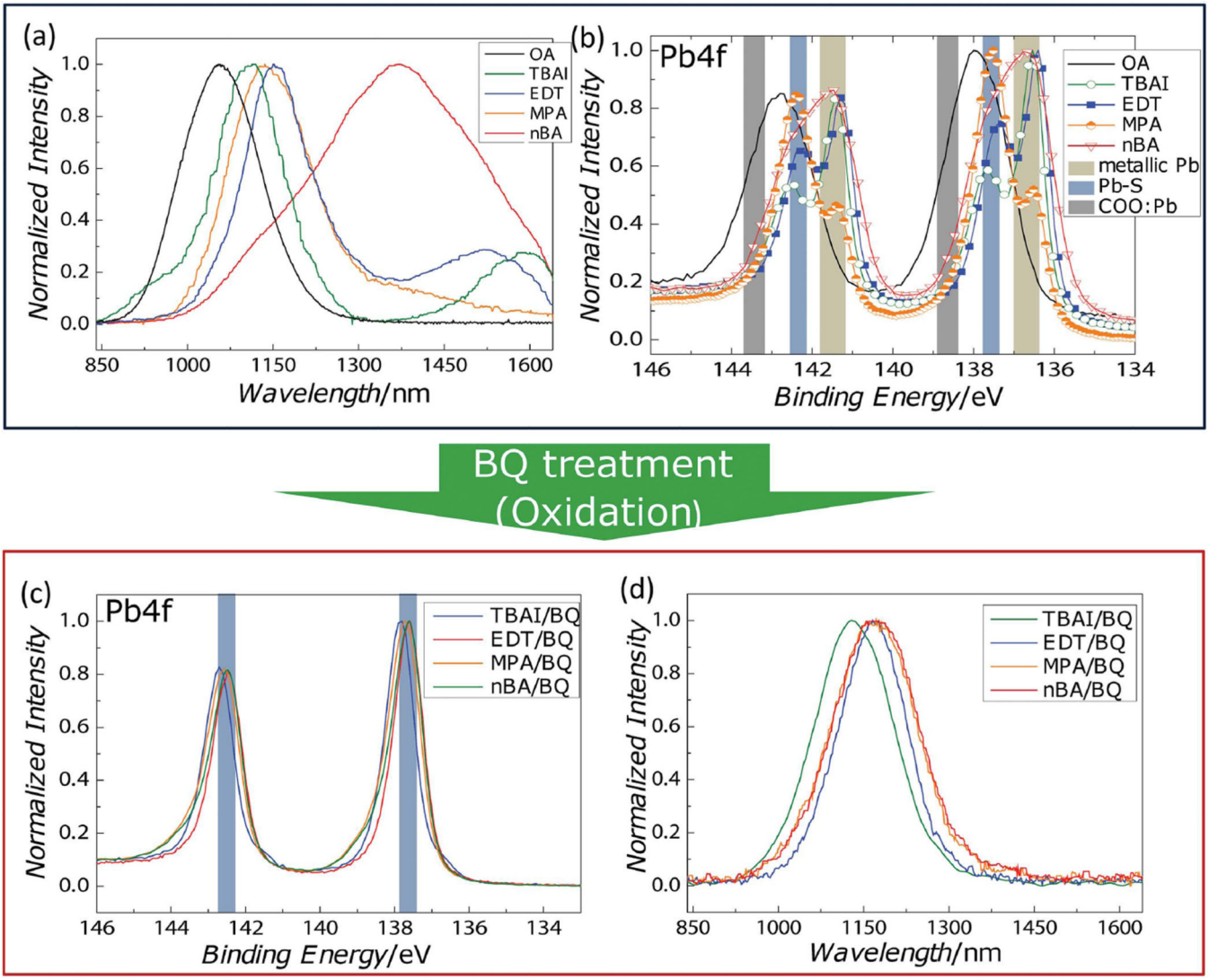


**Figure 1.**

a) PL from PbS QD thin films with different ligands—OA (black), TBAI (green), EDT (blue), MPA (orange), and nBA (red) and b) XPS on the Pb 4f feature for the same samples. The binding energies of metallic Pb, Pb–S, and COO:Pb are highlighted. c) XPS and d) PL measurements of ligand-exchanged PbS QD thin films following oxidation with BQ.

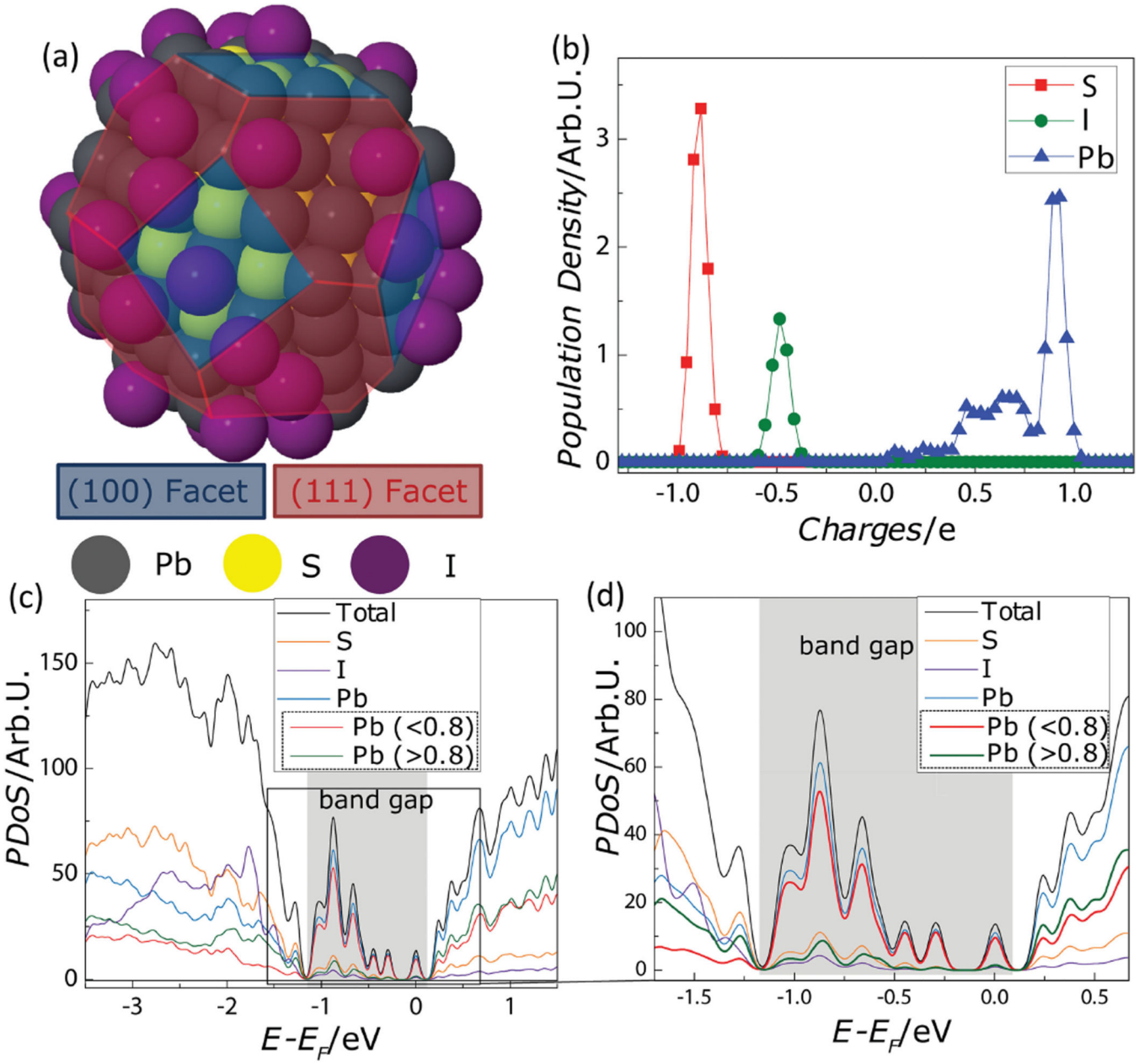


**Figure 2.**

a) The truncated octahedron shape of the model PbS QD used for the DFT calculations. b) Bader charge analysis gives the charge distribution for each element—Pb (blue), S(red), and I (green). c) The DoS (total, black) from DFT, broken into PDoS for each chemical species —S (orange), I (purple), and all Pb (blue). The PDoS of Pb further subdivided— contributions from under-charged Pb atoms (<0.8, red) and Pb atoms with a charge greater than 0.8 (green). d) An enlarged view (c) highlighting the DoS near the bandgap.

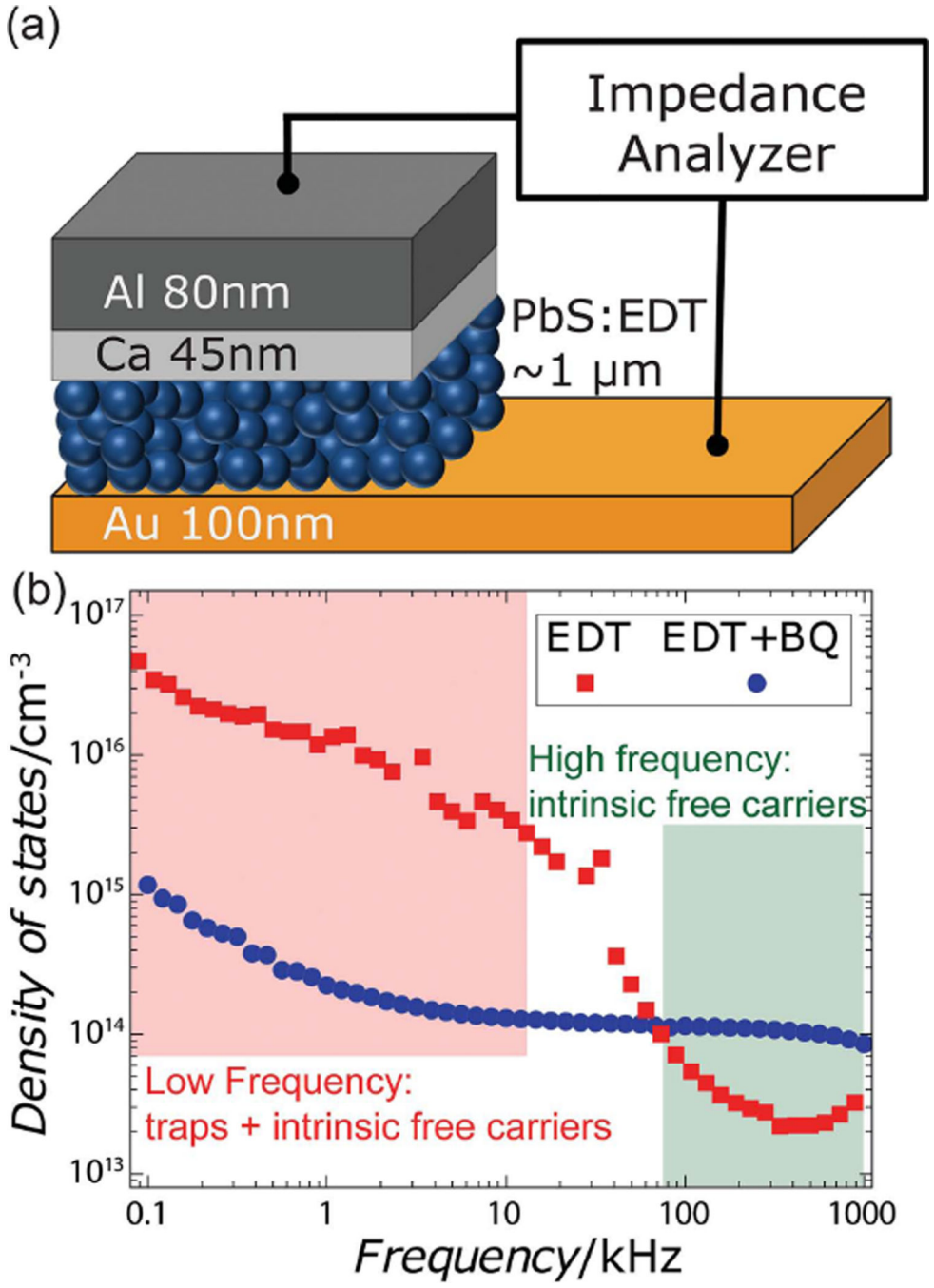


**Figure 3.**

a) A schematic of the Schottky diodes used for the DLCP measurements. b) DLCP measurement of the density of states of EDT-treated PbS films with and without the BQ treatment. The low-frequency regime (red box) includes contributions from carriers interacting with conductive and trap states, while the high-frequency regime (green box) gives the density of conductive states only.

**Table 1**

The atomic ratios of PbS QDs used in this work. Experimental data for the Pb-to-S ratio are obtained using WDS, and the I-to-Pb in TBAI-treated PbS QD thin films is measured using XPS. We include the ratios for the simulated QD used in DFT calculations for comparison.

| Samples | I/Pb ratio | Pb/S ratio |
|---|---|---|
| PbS:OA | n.a. | 1.58 ± 0.08 |
| PbS:TBAI | 0.336 ± 0.010 | 1.51 ± 0.14 |
| PbS:TBAI/BQ | 0.353 ± 0.016 | 1.45 ± 0.04 |
| Simulated PbS QDs | 0.302 | 1.47 |